Compressive Imaging by Generalized Total Variation Minimization

Jie Yan and Wu-Sheng Lu
Department of Electrical and Computer Engineering
University of Victoria
Victoria, BC, Canada V8W 3P6
jyan@ece.uvic.ca, wslu@ece.uvic.ca

***Abstract*—Encouraged by performance enhancement obtained using ℓ_p-minimization (with $p < 1$) relative to that of ℓ_1-minimization in compressive sensing, we present an algorithm for the reconstruction of digital images from undersampled measurements, where the concept of conventional TV is extended to a generalized TV (GTV) that involves pth power (with $p < 1$) of the discretized gradient of the image. To deal with the nonconvex issue arising from this new formulation, weighted TV (WTV) is introduced and an iterative reweighting technique is applied so that the algorithm is carried out in a convex setting. In addition, the Split Bregman method is reformulated in a major way so as to solve the WTV minimization problem involved. Numerical examples are included to demonstrate significant performance gain by the proposed GTV minimization method.**

I. Introduction

Compressive imaging (CI) is an important branch of compressive sensing (CS). The design of efficient CI systems remains a challenging problem as it involves a large amount of data, which has far-reaching implications for the complexity of the optical design, calibration, data storage and computational burden. A step towards overcoming the memory requirements is accomplished recently in [1], [2] by employing a separable sensing matrix. In [1], a two-dimensional separable sensing operator is used to reduce the storage of matrices of size $m^2 \times n^2$ produced by the Kronecker product of two $m \times n$ matrices. In addition, TV minimization using a Split Bregman approach with a separable sensing operator is studied in [3].

The exact formulation of the CI optimization problem depends on application. In this paper, we focus on the application of CI to sparse magnetic resonance imaging (MRI). The general form for the sparse MRI reconstruction problem is presented and discussed in [4]–[6]. Suppose we want to recover an MRI image $\mathbf{U} \in \mathbb{R}^{n \times n}$ based on randomized Fourier samples. When a TV sparsifying transform is considered, the optimization model can be expressed as

$$\min_{\mathbf{U}} \ \mathrm{TV}(\mathbf{U}) \quad \text{s.t.} \quad \|\mathbf{R} \circ (\mathcal{F}\mathbf{U}) - \mathbf{B}\|_F^2 < \sigma^2 \tag{1}$$

where $\mathcal{F}$ is the 2-D Fourier transform operator, $\mathbf{R}$ is a random sampling matrix whose entries are either 1 or 0, $\mathbf{B}$ corresponds to the observed "k-space" data [7], σ is the variance of the signal noise, and symbol $\circ$ denotes entrywise product between two matrices. It was shown in [8] that using a Bregman iteration technique, problem (1) can be reduced to a sequence of unconstrained problems that can be solved using the Split Bregman technique [7]. We stress that unlike other formulations presented in the literature, in problem (1) images are regarded as matrix variables instead of column-stacked vectors. Such formulation implicitly applies the separable sensing operator [1], [3] which facilitates efficient analysis, hence reduces storage complexity and makes fast computation possible. The matrix-based analysis of TV regularization model and its application to compressive imaging are the main contributions of this paper.

In [9], it is demonstrated that the standard TV can be generalized to a pth-power TV with $0 \le p \le 1$, and the generalized TV (GTV) regularized least squares problem produces improved denoising performance. In this paper, the GTV regularizer is applied to the Fourier-based MRI reconstruction problem, as a result we have to deal with a nonconvex model. Unlike the ℓ_1 or ℓ_p (with $p < 1$) regularization [10], [11], the algorithm proposed in this paper solves GTV-regularized optimization problem that turns out to perform better than existing algorithms in preserving image edges.

II. TV, Generalized TV and Weighted TV with Matrix Representations

The discretized anisotropic and isotropic total variation (TV) of images are defined and discussed in [12]. Since both TVs are found to yield similar reconstruction results with the performance often slightly in favor of the anisotropic one (see [9]), our analysis will be carried out using anisotropic type of TV.

TV of a digital image $\mathbf{U} \in \mathbb{R}^{n \times n}$ is defined as [12]

$$\begin{aligned}\mathrm{TV}(\mathbf{U}) = &\sum_{i=1}^{n-1}\sum_{j=1}^{n-1} \left(|U_{i,j} - U_{i+1,j}| + |U_{i,j} - U_{i,j+1}|\right) \\ &+ \sum_{i=1}^{n-1} |U_{i,n} - U_{i+1,n}| + \sum_{j=1}^{n-1} |U_{n,j} - U_{n,j+1}|\end{aligned} \tag{2}$$

The TV can be expressed with simple matrix operations. Given image $\mathbf{U} \in R^{n \times n}$, we define $\mathbf{D} \in R^{n \times n}$ as a circulant matrix with the first row $[1 \ -1 \ 0 \ \cdots \ 0]$. Under the periodic boundary condition, it can be verified that the TV of $\mathbf{U}$ can be expressed as

$$\mathrm{TV}(\mathbf{U}) = \|\mathbf{D}\mathbf{U}\|_1 + \|\mathbf{U}\mathbf{D}^T\|_1$$

where $\|\mathbf{X}\|_1$ denotes the sum of magnitudes of all the entries in $\mathbf{X}$, i.e., $\sum |x_{i,j}|$. It follows that the generalized pth power total variation, denoted as TV_p (see [9]), can be written as

$$\mathrm{TV}_p(\mathbf{U}) = \|\mathbf{D}\mathbf{U}\|_p + \|\mathbf{U}\mathbf{D}^T\|_p \tag{3}$$

with $0 \leq p \leq 1$. Note that $\|\mathbf{X}\|_p$ resembles but slightly differs from an ℓ_p norm. Specifically, it is the sum of pth power magnitudes of all the entries in $\mathbf{X}$, i.e., $\sum |x_{i,j}|^p$. The performance improvement using an ℓ_p norm over the ℓ_1 norm established in [13], [14] inspired us to investigate the generalized total variation, TV_p, for compressive sensing image recovery.

With TV_p defined, we consider the optimization model

$$\min_{\mathbf{U}} \ \text{TV}_p(\mathbf{U}) \ \ \text{s.t.} \ \ \|\mathbf{R} \circ (\mathcal{F}\mathbf{U}) - \mathbf{B}\|_{\text{F}}^2 \leq \sigma^2 \tag{4}$$

which may be regarded as a generalization of model (1) for the reason that the regularizer TV_p promotes a sparser TV when p is less than one. However, with $p < 1$ problem (4) is nonconvex. To deal with this nonconvexity, the idea for weighted TV (WTV) is introduced as

$$\text{TV}_{\text{w}}(\mathbf{U}) = \|\mathbf{W}_x \circ (\mathbf{D}\mathbf{U})\|_1 + \|\mathbf{W}_y \circ (\mathbf{U}\mathbf{D}^T)\|_1 \tag{5}$$

where $\circ$ is the Hadamard product operator, and $\mathbf{W}_x$ and $\mathbf{W}_y$ are weights matrices along the horizontal and vertical direction respectively. As will become transparent in Algorithm 1 below, WTV with properly chosen weights facilitates an excellent convex approximation of the nonconvex objective $\text{TV}_p(\mathbf{U})$.

III. Power-Iterative Reweighting Strategy

In theory, solving (4) with $p = 0$ promotes the solution with the sparsest TV. To approach the solution of a TV_0-regularized optimization problem, we adopt a power-iterative strategy similar to [14] by gradually reducing the power p while updating the weights and solving a WTV-regularized problem at each iteration. The power-iterative strategy not only properly updates the weights to approach the corresponding TV_p minimization, but also provides convex WTV-regularized problem with a good initial state obtained from the previous iteration. As a result, the WTV-regularized problem is found to converge considerably faster.

In what follows, we denote by $\mathbf{1}$ the matrix with each of its element one, by $|\mathbf{X}|^{.p}$ a matrix whose (i,j)th entry is $|x_{i,j}|^p$, and by $\circ/$ the pointwise division. The steps of the power-iterative strategy are summarized in Algorithm 1. We remark that via the reweighting formula (7), $\text{TV}_{\text{w}}(\mathbf{U})$ essentially becomes $\text{TV}_p(\mathbf{U})$ for $\mathbf{U}$ in a neighborhood of iterate $\mathbf{U}^{(l)}$. The parameter ϵ in (7) is a small constant to prevent the weights from being zero. In this way, nonconvex minimization of $\text{TV}_p(\mathbf{U})$ can practically be achieved by a series of convex minimization of $\text{TV}_{\text{w}}(\mathbf{U})$.

Algorithm 1 Power-Iterative Strategy for TV_p Minimization

1: Set $p = 1$, $l = 1$, $\mathbf{W}_x = \mathbf{W}_y = \mathbf{1}$.

2: Solve the WTV-regularized problem for $\mathbf{U}^{(l)}$

$$\min_{\mathbf{U}} \ \text{TV}_{\text{w}}(\mathbf{U}) \ \ \text{s.t.} \ \ \|\mathbf{R} \circ (\mathcal{F}\mathbf{U}) - \mathbf{B}\|_{\text{F}}^2 < \sigma^2 \tag{6}$$

3: Terminate if $p = 0$; otherwise, set $p = p - 0.1$ and update the weights $\mathbf{W}_x$ and $\mathbf{W}_y$ as

$$\mathbf{W}_x = |\mathbf{D}\mathbf{U}^{(l)} + \epsilon|^{.p-1}, \ \mathbf{W}_y = |\mathbf{U}^{(l)}\mathbf{D}^T + \epsilon|^{.p-1} \tag{7}$$

Then set $l = l + 1$ and repeat from step 2.

IV. Solving Problem (6)

The analysis has led to a WTV-regularized problem as seen in (6). We propose to solve the problem using a Split Bregman [7] approach, but with important changes as will be described in the following. Unlike vector operations in the literature, the entire analysis presented below is carried out in terms of matrix operations.

A. Split Bregman Type Iteration

First, we apply the Bregman iteration [8] to (6) which reduces the problem to

$$\mathbf{U}^{(k+1)} = \underset{\mathbf{U}}{\text{argmin}} \, \text{TV}_{\text{w}}(\mathbf{U}) + \frac{\mu}{2}\|\mathbf{R} \circ (\mathcal{F}\mathbf{U}) - \mathbf{B}^{(k)}\|_{\text{F}}^2 \tag{8a}$$

$$\mathbf{B}^{(k+1)} = \mathbf{B}^{(k)} + \mathbf{B} - \mathbf{R} \circ (\mathcal{F}\mathbf{U}^{(k+1)}) \tag{8b}$$

With Eq. (5), problem (8) can be expressed as

$$\begin{aligned} \mathbf{U}^{(k+1)} = \underset{\mathbf{U}}{\text{argmin}} & \|\mathbf{W}_x \circ (\mathbf{D}\mathbf{U})\|_1 + \|\mathbf{W}_y \circ (\mathbf{U}\mathbf{D}^T)\|_1 \\ & + \frac{\mu}{2}\|\mathbf{R} \circ (\mathcal{F}\mathbf{U}) - \mathbf{B}^{(k)}\|_{\text{F}}^2 \end{aligned} \tag{9a}$$

$$\mathbf{B}^{(k+1)} = \mathbf{B}^{(k)} + \mathbf{B} - \mathbf{R} \circ (\mathcal{F}\mathbf{U}^{(k+1)}) \tag{9b}$$

Next, a splitting strategy applied to (9a) leads to the formulation

$$\min_{\mathbf{U}} \|\mathbf{W}_x \circ \mathbf{D}_x\|_1 + \|\mathbf{W}_y \circ \mathbf{D}_y\|_1 + \frac{\mu}{2}\|\mathbf{R} \circ (\mathcal{F}\mathbf{U}) - \mathbf{B}^{(k)}\|_{\text{F}}^2 \tag{10a}$$

$$\text{s.t. } \mathbf{D}_x = \mathbf{D}\mathbf{V}, \mathbf{D}_y = \mathbf{V}\mathbf{D}^T, \mathbf{U} = \mathbf{V} \tag{10b}$$

Note that in (10) we have applied the Split Bregman technique [7] for the splitting $\mathbf{D}_x = \mathbf{D}\mathbf{V}$ and $\mathbf{D}_y = \mathbf{V}\mathbf{D}^T$, and introduced an additional split as $\mathbf{U} = \mathbf{V}$ which guarantees that this is, in fact, the same one variable; however such a split allows us to decompose a most expensive step of the algorithm into two much simpler steps [3].

Applying Bregman method again to (10) to enforce constraints in (10b), we are led to the following problem with respect to $\{\mathbf{U}, \mathbf{V}, \mathbf{D}_x, \mathbf{D}_y\}$

$$\begin{aligned} \min \ & \|\mathbf{W}_x \circ \mathbf{D}_x\|_1 + \|\mathbf{W}_y \circ \mathbf{D}_y\|_1 + \frac{\mu}{2}\|\mathbf{R} \circ (\mathcal{F}\mathbf{U}) - \mathbf{B}^{(k)}\|_{\text{F}}^2 \\ & + \frac{\lambda}{2}\|\mathbf{D}_x - \mathbf{D}\mathbf{V} - \mathbf{E}_x^{(h)}\|_{\text{F}}^2 + \frac{\lambda}{2}\|\mathbf{D}_y - \mathbf{V}\mathbf{D}^T - \mathbf{E}_y^{(h)}\|_{\text{F}}^2 \\ & + \frac{\nu}{2}\|\mathbf{U} - \mathbf{V} - \mathbf{G}^{(h)}\|_{\text{F}}^2 \end{aligned}$$

where $\mathbf{E}_x^{(h)}$, $\mathbf{E}_y^{(h)}$ and $\mathbf{G}^{(h)}$ are updated by Bregman iterations. In the hth iteration, we solve four subproblems as

$$\begin{aligned} \mathbf{U}^{(h+1)} = \underset{\mathbf{U}}{\text{argmin}} & \frac{\mu}{2}\|\mathbf{R} \circ (\mathcal{F}\mathbf{U}) - \mathbf{B}^{(k)}\|_{\text{F}}^2 \\ & + \frac{\nu}{2}\|\mathbf{U} - \mathbf{V}^{(h)} - \mathbf{G}^{(h)}\|_{\text{F}}^2 \end{aligned} \tag{11}$$

$$\begin{aligned} \mathbf{V}^{(h+1)} = & \underset{\mathbf{V}}{\text{argmin}} \frac{\nu}{2}\|\mathbf{V} - \mathbf{U}^{(h+1)} + \mathbf{G}^{(h)}\|_{\text{F}}^2 \\ & + \frac{\lambda}{2}\|\mathbf{D}\mathbf{V} + \mathbf{E}_x^{(h)} - \mathbf{D}_x^{(h)}\|_{\text{F}}^2 + \frac{\lambda}{2}\|\mathbf{V}\mathbf{D}^T + \mathbf{E}_y^{(h)} - \mathbf{D}_y^{(h)}\|_{\text{F}}^2 \end{aligned} \tag{12}$$

$$\mathbf{D}_x^{(h+1)} = \underset{\mathbf{D}_x}{\operatorname{argmin}} \|\mathbf{W}_x \circ \mathbf{D}_x\|_1 + \frac{\lambda}{2}\|\mathbf{D}_x - \mathbf{D}\mathbf{V}^{(h+1)} - \mathbf{E}_x^{(h)}\|_{\mathrm{F}}^2 \tag{13a}$$

$$\mathbf{D}_y^{(h+1)} = \underset{\mathbf{D}_y}{\operatorname{argmin}} \|\mathbf{W}_y \circ \mathbf{D}_y\|_1 + \frac{\lambda}{2}\|\mathbf{D}_y - \mathbf{V}^{(h+1)}\mathbf{D}^T - \mathbf{E}_y^{(h)}\|_{\mathrm{F}}^2 \tag{13b}$$

where $\mathbf{G}^{(h)}$, $\mathbf{E}_x^{(h)}$ and $\mathbf{E}_y^{(h)}$ are updated as

$$\mathbf{G}^{(h+1)} = \mathbf{G}^{(h)} + \mathbf{V}^{(h+1)} - \mathbf{U}^{(h+1)} \tag{14a}$$

$$\mathbf{E}_x^{(h+1)} = \mathbf{E}_x^{(h)} + \mathbf{D}\mathbf{V}^{(h+1)} - \mathbf{D}_x^{(h+1)} \tag{14b}$$

$$\mathbf{E}_y^{(h+1)} = \mathbf{E}_y^{(h)} + \mathbf{V}^{(h+1)}\mathbf{D}^T - \mathbf{D}_y^{(h+1)} \tag{14c}$$

Typically, it takes a small number of iterations of (11), (12), (13) and (14) for the algorithm to converge.

The problems (13a) and (13b) can be solved by soft shrinkage as the unknowns are separate from each other:

$$\mathbf{D}_x^{(h+1)} = \mathcal{T}_{\mathbf{W}_x/\lambda}(\mathbf{D}\mathbf{V}^{(h+1)} + \mathbf{E}_x^{(h)}) \tag{15a}$$

$$\mathbf{D}_y^{(h+1)} = \mathcal{T}_{\mathbf{W}_y/\lambda}(\mathbf{V}^{(h+1)}\mathbf{D}^T + \mathbf{E}_y^{(h)}) \tag{15b}$$

where soft shrinkage operator $\mathcal{T}$ applies pointwisely as

$$\mathcal{T}_{w_{i,j}/\lambda}(z) = \operatorname{sgn}(z) \cdot \max\{|z| - w_{i,j}/\lambda, 0\} \tag{16}$$

B. Solving Problems (11) and (12)

Solving problems (11) and (12) are far from trivial. To this end, we write the 1st-order optimality condition of (11) as

$$\mu\mathcal{F}^T\mathbf{R} \circ \mathcal{F}\mathbf{U} + \nu\mathbf{U} = \mu\mathcal{F}^T\mathbf{R} \circ \mathbf{B}^k + \nu(\mathbf{V}^{(h)} + \mathbf{G}^{(h)}) \tag{17}$$

Multiplying both sides of (17) by $\mathcal{F}$ and applying the orthogonality of Fourier transform, we have

$$\mu\mathbf{R} \circ \mathcal{F}\mathbf{U} + \nu\mathcal{F}\mathbf{U} = \mu\mathbf{R} \circ \mathbf{B}^k + \nu\mathcal{F}(\mathbf{V}^{(h)} + \mathbf{G}^{(h)}) \tag{18}$$

Furthermore, the Fourier transform of $\mathbf{U}$ can be derived as

$$\mathcal{F}\mathbf{U} = \Big[\mu\mathbf{R} \circ \mathbf{B}^k + \nu\mathcal{F}(\mathbf{V}^{(h)} + \mathbf{G}^{(h)})\Big] \circ / \ (\mu\mathbf{R} + \nu) \tag{19}$$

Finally, by taking the inverse Fourier transform of (19), the solution of (11) has the following representation

$$\mathbf{U}^{(h+1)} = \mathcal{F}^T \left\{ \Big[\mu\mathbf{R} \circ \mathbf{B}^k + \nu\mathcal{F}(\mathbf{V}^{(h)} + \mathbf{G}^{(h)})\Big] \circ / \ (\mu\mathbf{R} + \nu) \right\} \tag{20}$$

To solve problem (12), we use matrix calculus to write its first-order optimality condition as

$$\nu\mathbf{V} + \lambda\mathbf{D}^T\mathbf{D}\mathbf{V} + \lambda\mathbf{V}\mathbf{D}^T\mathbf{D} = \mathbf{C}^{(h)} \tag{21}$$

where

$$\begin{aligned} \mathbf{C}^{(h)} &= \nu(\mathbf{U}^{(h+1)} - \mathbf{G}^{(h)}) \\ &\quad + \lambda\mathbf{D}^T(\mathbf{D}_x^{(h)} - \mathbf{E}_x^{(h)}) + \lambda(\mathbf{D}_y^{(h)} - \mathbf{E}_y^{(h)})\mathbf{D} \end{aligned} \tag{22}$$

Due to the periodic boundary condition, matrix $\mathbf{D}$ is circulant and can be diagonalized by the 2-D Fourier transform as $\mathbf{D} = \mathcal{F}^T\mathbf{\Lambda}\mathcal{F}$ [15], [16]. Substituting into (21), we have

$$\nu\mathbf{V} + \lambda\mathcal{F}^T\mathbf{\Lambda}^*\mathbf{\Lambda}\mathcal{F}\mathbf{V} + \lambda\mathbf{V}\mathcal{F}^T\mathbf{\Lambda}^*\mathbf{\Lambda}\mathcal{F} = \mathbf{C}^{(h)} \tag{23}$$

which can be further reduced to

$$\nu\tilde{\mathbf{V}} + \lambda(\mathbf{T}\tilde{\mathbf{V}} + \tilde{\mathbf{V}}\mathbf{T}) = \mathcal{F}\mathbf{C}^{(h)}\mathcal{F}^T \tag{24}$$

where $\tilde{\mathbf{V}} = \mathcal{F}\mathbf{V}\mathcal{F}^T$ and $\mathbf{T} = \mathbf{\Lambda}^*\mathbf{\Lambda}$. It follows that

$$\mathbf{T}\tilde{\mathbf{V}} = \mathbf{T}_r \circ \tilde{\mathbf{V}}, \ \ \tilde{\mathbf{V}}\mathbf{T} = \mathbf{T}_c \circ \tilde{\mathbf{V}}$$

where $\mathbf{T}_r$ has each element in its ith row as $T_{i,i}$ and $\mathbf{T}_c$ has each element in its ith column as $T_{i,i}$. Thus, (24) gives

$$(\nu + \lambda\mathbf{T}_r + \lambda\mathbf{T}_c) \circ \tilde{\mathbf{V}} = \mathcal{F}\mathbf{C}^{(h)}\mathcal{F}^T \tag{25}$$

In consequence, we obtain solution of (12) as

$$\mathbf{V}^{(h+1)} = \mathcal{F}^T \Big\{ (\mathcal{F}\mathbf{C}^{(h)}\mathcal{F}^T) \circ / (\nu + \lambda\mathbf{T}_r + \lambda\mathbf{T}_c) \Big\} \mathcal{F} \tag{26}$$

The algorithm for solving the WTV-regularized problem (6) is summarized as Algorithm 2.

Algorithm 2 Algorithm for WTV-regularized problem (6)

1: Set μ, λ and ν. Set maximum inner and outer iteration number K and H. Initialize $\mathbf{B}^{(0)}$, $\mathbf{V}^{(0)}$, $\mathbf{G}^{(0)}$, $\mathbf{D}_x^{(0)}$, $\mathbf{D}_y^{(0)}$, $\mathbf{E}_x^{(0)}$ and $\mathbf{E}_y^{(0)}$.
2: **for** $k = 0, ..., K-1$ **do**
3:   **for** $h = 0, ..., H-1$ **do**
4:     Compute $\mathbf{U}^{(h+1)}$, $\mathbf{V}^{(h+1)}$, $\mathbf{D}_x^{(h+1)}$, $\mathbf{D}_y^{(h+1)}$ by Eqs. (20), (26) and (15), respectively. Update $\mathbf{G}^{(h+1)}$, $\mathbf{E}_x^{(h+1)}$, $\mathbf{E}_y^{(h+1)}$ through Eq (14).
5:   **end for**
6:   Set $\mathbf{U}^{(k+1)} = \mathbf{U}^{(H)}$. Update $\mathbf{B}^{(k+1)}$ by Eq (8b).
7: **end for**

V. Performance Evaluation

A. MRI of the Shepp-Logan Phantom

The Shepp-Logan phantom is a standard test image and serves as a model of a human head in image reconstruction algorithms [17], and is used widely by researchers in tomography. In our experiment, a normalized Shepp-Logan phantom of size 256×256, was measured at 2521 locations (as low as 3.85%) in the 2D Fourier plane (k-space); the sampling pattern was a star-shaped pattern consisting of only 10 radial lines, see Fig. 1(a). Based on the star-shaped Fourier samples, a minimum ℓ_2 norm reconstruction is shown in Fig. 1(b). To apply Algorithm 1, we set $p = 1$ and $\mathbf{W}_x$ and $\mathbf{W}_y$ as $\mathbf{1}$. In each round of iteration, problem (6) was solved by Algorithm 2. We set parameters μ, λ and ν to 5, the inner and outter iterations to $H = 10$ and $K = 100$, and $\mathbf{B}^{(0)}$, $\mathbf{V}^{(0)}$, $\mathbf{G}^{(0)}$, $\mathbf{D}_x^{(0)}$, $\mathbf{D}_y^{(0)}$, $\mathbf{E}_x^{(0)}$, $\mathbf{E}_y^{(0)}$ to zero matrices. The minimizer of problem (6) was then used to update $\mathbf{W}_x$ and $\mathbf{W}_y$ for the next round when $p = 0.9$ in Algorithm 1. It is important to remark that starting from the 2nd round in solving problem (6), $\mathbf{B}^{(0)}$, $\mathbf{V}^{(0)}$, $\mathbf{G}^{(0)}$, $\mathbf{D}_x^{(0)}$, $\mathbf{D}_y^{(0)}$, $\mathbf{E}_x^{(0)}$ and $\mathbf{E}_y^{(0)}$ were initialized using the most recent iterates from the last cycle. The steps were carried on for $p = 0.8, 0.7, 0.6, ...$ and so forth until the result for $p = 0$ is achieved.

It took a PC laptop with a 2.67 GHz Intel dual-core processor 770.7 seconds to produce the reconstructed phantom for $p = 0$ shown in Fig. 1(d) with a signal to noise (SNR) ratio as 16.3 dB. For a fair comparison, we set $\mathbf{W}_x = \mathbf{W}_y = \mathbf{1}$, and minimize problem (6) by Algorithm 2 with $K = 1100$. The computational time was found to be 756.8s. The solution simply corresponds to the conventional TV minimization recovery

(1) (see Fig. 1(c)) with the maximum SNR found to be 8.8 dB. Therefore, using the proposed method to approach the TV_0 solution, we have observed better reconstruction performance relative to the conventional TV minimization.

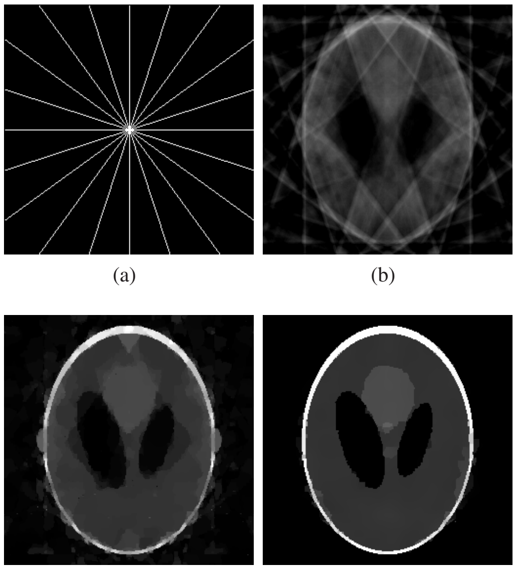

(a) (b) (c) (d)

Fig. 1: (a) Star-shaped sampling pattern (b) Minimum energy reconstruction (c) Minimum TV reconstruction (d) Minimum GTV reconstruction with $p = 0$

B. Compressive Imaging of Natural Images

To further examine the proposed GTV minimization algorithm, we extend the simulation to compressive sensing of several natural images - `cameraman`, `building`, `milk` and `jet`. Each test image of size 256 by 256 was measured at 13107 random locations (i.e., 20% of size of image) in the 2D Fourier plane.

The parameter setting was the same as in Sec. V-A. The power iterative technique was also applied to reduce the power p from 1 to 0 with a 0.1 step each time, in order to ensure a decent initial point. Reconstruction performance of the proposed GTV ($p = 0$) algorithm compared with TV based minimization was illustrated in Table I.

Original Images	cameraman	building	milk	jet
TV	14.3	15.2	12.1	16.2
GTV ($p = 0$)	19.5	18.3	14.5	18.3

TABLE I: SNRs (in dB) of reconstructed images by TV minimization and the proposed GTV algorithm for images `cameraman`, `building`, `milk` and `jet`.

It was found that the images reconstructed using the proposed GTV minimization method possess consistently higher SNRs than those from the conventional minimum TV reconstruction, which demonstrates that the proposed GTV minimization algorithm has an edge on the conventional TV model in reconstructing images from compressive measurements.

VI. Conclusion

An algorithm for generalized TV minimization for compressive imaging has been proposed. In particular, a weighted TV-regularized problem has been solved in the Split Bregman framework with additional splitting technique. The algorithm includes a power-iterative strategy that gradually reduces the power p from 1 to 0. The algorithm has been simulated on a variety of medical and natural images, and found to outperform the conventional TV minimization method in terms of the reconstructed image quality.

References

[1] Y. Rivenson and A. Stern, "Compressed imaging with a separable sensing operator," *Signal Processing Letters, IEEE*, vol. 16, no. 6, pp. 449–452, 2009.

[2] M. F. Duarte and R. G. Baraniuk, "Kronecker compressive sensing," *Image Processing, IEEE Trans.*, vol. 21, no. 2, pp. 494–504, 2012.

[3] S. L. Shishkin, H. Wang, and G. S. Hagen, "Total variation minimization with separable sensing operator," in *Image and Signal Processing*. Springer, 2010, pp. 86–93.

[4] M. Lustig, D. Donoho, and J. M. Pauly, "Sparse MRI: The application of compressed sensing for rapid MR imaging," *Magnetic resonance in medicine*, vol. 58, no. 6, pp. 1182–1195, 2007.

[5] T.-C. Chang, L. He, and T. Fang, "MR image reconstruction from sparse radial samples using Bregman iteration," in *Proceedings of the 13th Annual Meeting of ISMRM, Seattle*, 2006, p. 696.

[6] K. Koh, S.-J. Kim, and S. P. Boyd, "An interior-point method for large-scale l1-regularized logistic regression." *Journal of Machine learning research*, vol. 8, no. 8, pp. 1519–1555, 2007.

[7] T. Goldstein and S. Osher, "The split Bregman method for l1 regularized problems," *SIAM Journal on Imaging Sciences*, vol. 2, no. 2, pp. 323–343, 2009.

[8] W. Yin, S. Osher, D. Goldfarb, and J. Darbon, "Bregman iterative algorithms for l1-minimization with applications to compressed sensing," *SIAM J. Imaging Sci*, vol. 1, no. 1, pp. 143–168, 2008.

[9] J. Yan and W.-S. Lu, "Image denoising by generalized total variation regularization and least squares fidelity," *Multidimensional Systems and Signal Processing*, pp. 1–24, 2013. [Online]. Available: http://dx.doi.org/10.1007/s11045-013-0255-2

[10] R. Chartrand and W. Yin, "Iteratively reweighted algorithms for compressive sensing," in *ICASSP 2008*, pp. 3869–3872.

[11] R. Chartrand, "Fast algorithms for nonconvex compressive sensing: MRI reconstruction from very few data," in *Biomedical Imaging: From Nano to Macro, 2009. ISBI'09. IEEE International Symposium on*. IEEE, 2009, pp. 262–265.

[12] A. Beck and M. Teboulle, "Fast gradient-based algorithms for constrained total variation image denoising and deblurring problems," *Image Processing, IEEE Trans.*, vol. 18, no. 11, pp. 2419–2434, 2009.

[13] R. Chartrand, "Exact reconstruction of sparse signals via nonconvex minimization," *Signal Processing Letters, IEEE*, vol. 14, no. 10, pp. 707–710, 2007.

[14] J. Yan and W.-S. Lu, "Power-iterative strategy for ℓ_p-ℓ_2 optimization for compressive sensing: towards global solution," in *Asilomar 2011*, Pacific Grove, CA, Nov. 2011.

[15] M. K. Ng, R. H. Chan, and W.-C. Tang, "A fast algorithm for deblurring models with Neumann boundary conditions," *SIAM Journal on Scientific Computing*, vol. 21, no. 3, pp. 851–866, 1999.

[16] W. Yin, S. Morgan, J. Yang, and Y. Zhang, "Practical compressive sensing with Toeplitz and circulant matrices," in *Proc. SPIE*, vol. 7744, 2010, p. 77440K.

[17] C. G. Koay, J. E. Sarlls, and E. Özarslan, "Three-dimensional analytical magnetic resonance imaging phantom in the Fourier domain," *Magnetic Resonance in Medicine*, vol. 58, no. 2, pp. 430–436, 2007.